An interpretation of the hydrogen inhibiting effect on chemical vapor deposition of pyrocarbon obtained by propane pyrolysis.

I. Ziegler-Devin[*1,2], R. Fournet[1], R. Lacroix[1], P. M. Marquaire[1]

[1]*Université de Lorraine, LRGP, UMR 3349, 1 rue Grandville, BP 20451, NANCY, F-54001, France*

[2]*Université de Lorraine, LERMAB, EA 4370, Faculté des Sciences et Technologies, F-54506 Vandoeuvre-lès-Nancy, France*

[*]CORRESPONDING AUTHOR

Dr Isabelle Ziegler-Devin
Université de Lorraine, LERMaB, EA 4370, Faculté des Sciences et Technologies, F-54506 Vandoeuvre-lès-Nancy, France
mail : isabelle.ziegler@univ-lorraine.fr
phone : + 33-383175121

Abstract

A detailed kinetic mechanism, based on elementary steps, modeling both pyrocarbon deposition on carbon fibers and gas phase composition obtained by propane pyrolysis has been proposed. This model, based on heterogeneous and homogeneous elementary steps is efficient to predict pyrocarbon deposition rate and gas phase composition when the influence of temperature (1173-1323 K), residence time (0.5-4 s), carbon surface fibers, and reactor inlet mixture is studied. In this paper, we discuss experimental and modeling results of hydrogen inhibiting effects on pyrocarbon deposit and gas phase composition during propane/hydrogen pyrolysis. Simulated results are coherent with experimental data when the pyrocarbon deposition rate is studied. Compared to pure propane chemical vapour deposition, the mole fractions of C_2 and C_4 gas phase species are not affected by an increasing of hydrogen inlet, whereas pyrocarbon deposition rate and mole fractions of C_3 and aromatic species decrease. These results also confirm, in accordance with the literature, that hydrogen inhibits highly the formation of pyrocarbon and aromatic species.

Keywords

Detailed kinetic modelling, elementary steps, pyrocarbon, gas chromatography, pyrolysis, perfectly stirred reactor

1. Introduction

Carbon/carbon composites are widely used as rocket nozzles and plane brakes in the aeronautic and space industries, where the use of materials with specific chemical and physical properties at high temperature is required. Such products are often prepared by densification of a fibrous preform with a pyrolytic matrix of carbon through a chemical vapor infiltration or deposition process (CVI/CVD). This process consists in the deposition of a

matrix of pyrocarbon on a substrate surface by thermal decomposition of gaseous hydrocarbons such as methane or propane [1-5], unsaturated species (ethylene, acetylene…) [6-7] or organic species [8] at high temperature and low pressure. The CVD/CVI of pyrocarbon from pyrolysis of a hydrocarbon precursor is a complex phenomenon which is still an object of scientific research despite it has been widely studied for several decades. Indeed, during the last few years, a significant number of experimental and modeling studies has been carried out in order to elucidate the chemistry of pyrocarbon deposition and to establish the most important parameters involved in the formation of pyrocarbon, as temperature, pressure, residence time or the ratio of the carbon fibers area and the volume of the gas phase (A/V) [1-10].

The aim of this paper is to complete the knowledge of the influence of hydrogen mole fraction in the gas phase on the deposition rate of pyrocarbon. Indeed, the study of the inhibition by hydrogen during the pyrocarbon deposition has been the object of several publications in the last years, but a detailed kinetic mechanism has never been used to understand this phenomenon.

This paragraph will focus on the literature related to the influence of the hydrogen mole fraction in the gas phase on pyrocarbon deposition rate and gas phase composition. According to Li et al. [11-13], hydrogen inhibits pyrocarbon deposition. The authors propose in their papers a global model based on the deposition of three gas phase species, which are ethylene, acetylene and benzene (figure 1).

Figure 1: Multi-step CVD and hydrogen inhibition of pyrocarbon from methane proposed by Li et al. [13].

Each kinetic rate of the three deposition reactions, which follows the Arrhenius law, is multiplied by a hydrogen inhibition function called “fi “, which is presented in table 1. A lumped surface model mechanism is proposed to describe the pyrolytic deposition from these three hydrocarbons. According to these authors, the deposition of ethylene, acetylene and benzene decreases when the mole fraction of hydrogen increases [12].

Table I: Hydrogen inhibition functions of a global deposition model proposed by Li et al. [13].

Becker et al. have also proposed a global modeling approach based on deposition reactions on active sites [14]. For instance, the deposition of acetylene consists in a combination of two reactions on two surface sites mentioned as ““C∝()”, one of these reactions is supposed to be irreversible whereas the other is reversible:

$$C_{\infty}() + C_xH_y \xrightarrow{k_{II}} C_{\infty}(H_y) \qquad \text{(I)}$$

$$C_{\infty}(H_y) \underset{k_{-IV}}{\overset{k_{IV}}{\rightleftarrows}} C_{\infty}() + \frac{y}{2}H_2 \qquad \text{(II)}$$

At constant acetylene partial pressure, the pyrocarbon formation rate “r” by acetylene deposition in inversely proportional to the partial pressure of hydrogen and so takes into account the inhibiting effect of H_2 (Equation 1).

$$r^{-1} = \left(\frac{1}{c\,k_{IV}} + \frac{1}{c\,k_{II}\,p_{C_XH_y}} + \frac{k_{-IV}}{c\,k_{II}\,k_{IV}\,p_{C_XH_y}} \right) p_{H2} \qquad (1)$$

The inhibition effect of hydrogen on pyrocarbon deposition rate is also demonstrated by the authors for deposition of other hydrocarbons such as methane.

Tang et al have also studied the effect of hydrogen on pyrocarbon deposition rate [15]. In their experimental conditions they have concluded that despite its inhibition on pyrocarbon deposition, H_2 is acting as a non-inert carrier gas, and it has positive effects on the densification of carbon fibers preforms when the control temperature is higher than 1173 K; but it has negative effects on the densification when the control temperature is as low as 1123 K.

Finally, the effect of hydrogen addition has been also studied in other conditions of carbon formation such as coke, soot, or diamond [16-18]. For instance, Frenklach has shown that the key role of the hydrogen addition in the diamond deposition process is to suppress the formation of aromatic species in the gas phase and thereby to prevent the formation and growth of non-diamond, graphitic phases on the deposition surface [18-19].

So whatever the studies are, it is well known and commonly accepted that hydrogen inhibits pyrocarbon deposition but also formation of soot or polycyclic aromatic hydrocarbon (PAH) as well; nevertheless the mechanism of this inhibition remains not clear. That's why in this work, a detailed kinetic mechanism, validated on experimental data, and describing both pyrocarbon and gas phase reactions is used to investigate the inhibition effect of hydrogen.

2. Experimental set up of this study

The experimental set-up used in this work has been described in details in previous publications ([5]; [20-23]). Chemical vapor deposition of pyrocarbon takes place in a perfectly stirred reactor at a temperature of 1273 K and a residence time of 1 second. The reactor is made of quartz and is composed of two parts: the half-spherical upper part (≈ 90 cm^3) contains an injection cross, composed of four small nozzles, and is located at its center. In this zone, pressure, temperature and composition of the gas phase are homogeneous [24]. The upper part also includes an annular preheating directly connected to the injection cross; it

allows the preheating of reactants at the reaction temperature in a short time compared to the reaction time. The lower part is a removable pierced cylinder on which a preform made of carbon fibers can be laid. The main advantage of this reactor is that the gaseous composition is the same in all its volume and also near the porous preform where the pyrocarbon deposition takes place; therefore, it is possible to know precisely the composition of the gas phase in the conditions of the pyrocarbon deposition.

Propane, hydrogen and nitrogen flows are introduced and controlled in the reactor by the mean of mass flow regulators provided by Bronkhorst. Temperature, which is isothermal in the reactor, is controlled by an oven tube furnace 79300 provided by Thermolyne, whereas the low pressure (< 3 kPa) is controlled by a vacuum pump and valves located at the exit of the reactor. Each experiment is carried out in the presence of a preform made of braided carbon fibers on which the pyrocarbon deposition takes place. The preform has an initial mass equal to 1.3 g and the contact area between carbon fibers and the gas phase is around 3960 cm^2. In this work, the pyrocarbon deposition is obtained by pyrolysis of a mixture of propane/hydrogen diluted in nitrogen; the propane mole fraction in the reactor inlet equals 10 % for all experiments. The mole fraction of hydrogen in the reactor ranges from 0 to 30%, the remaining fraction being composed of nitrogen (60 - 90%). By the mean of three gas-chromatographs (FID, TCD, MS detectors), 29 products (H_2, methane to pyrene) are quantified, whereas the pyrocarbon deposition rate is calculated by weighting the preform before and after 90 minutes of infiltration.

3. The modeling of pyrocarbon deposition and gas phase during propane pyrolysis

With the previous experimental conditions, the pyrolysis of propane produces pyrocarbon but also many gaseous species such as hydrogen, small hydrocarbons, aromatic and polyaromatic

hydrocarbons. The development of a detailed kinetic mechanism can be useful to determine the concentration of these species in different conditions of pyrolysis.

The mechanism used in this paper is composed of elementary steps which describe both gaseous and solid reactions (i.e. pyrocarbon formation) ; the main features are recalled below. Simulations are then performed using the Surface Chemkin package.

3.1 Gas phase reactions

The first part of the mechanism describing gaseous reactions of the propane pyrolysis is composed of 608 reversible elementary reactions and involves 193 molecules or radicals. This mechanism is described in details in the following references [21-22]. The reactions are composed of elementary steps such as initiation, H-abstraction, addition of unsaturated species, β-scission, ipso addition and termination.

The kinetics parameters used in the mechanism mainly come from literature. In the case of initiation or combination reactions, they are calculated with the software Kingas [25]. Finally when no data are available, especially for reactions of polyaromatic hydrocarbons, they are estimated by means of correlations between structure and reactivity of molecules [22]. The pressure dependence of some reactions involving small species is also taken into account by means of Troë parameters [26].

Concerning the thermochemical data used in the mechanism, they are mainly calculated by using Thergas software [27], otherwise they are found in the literature.

3.2 Surface reactions

The second part of the mechanism describing reactions of pyrocarbon deposit is comprised of 275 non-reversible elementary involving 63 surface sites. A detailed description of the mechanism can be found in the following reference [5].

Pyrocarbon formation is supposed to take place on the edges of basic structural units (BSU) of pyrocarbon. Pyrocarbon is formed when gaseous species are added to these sites and lead to the formation of new ring containing six atoms of carbon. These BSU present both armchair and zig-zag sites and it is supposed that 50% of surface sites are arm-chair like, the remaining half being zig-zag like.

Figure 2: Zig-zag and armchair surface sites.

To complete an armchair site into an aromatic ring composed of six carbon atoms, the addition of at least two carbon atoms is required. Whereas the formation of a six atoms ring from a zig-zag site needs at least three carbon atoms. In the mechanism, the lateral increase of these BSU is assumed to be chemically identical to the growth of gaseous aromatic species and is described with the same reactions that those used in the gas phase mechanism, that is, H-abstraction, addition of unsaturated species, β-scission, ipso addition, initiation and termination reactions. Then, the deposit of unsaturated molecules (acetylene, ethylene, propene, propadiene, propyne, styrene, phenylacetylene, benzene and naphthalene) and radicals (CH_3, C_2H, C_2H_3, C_2H_5 and phenyl radicals) is taken into account.

The kinetic data combined with these surface elementary steps, have been estimated by analogy with a gas phase "prototype" reaction, these two elementary processes must be close from a chemical point of view. More precisely, the reactions taking place at the edges of the BSU are supposed to be similar to gas phase reactions involving benzene (or its derivatives).

For example, an H abstraction between the edge of a BSU and a radical in the gas phase is supposed to be similar to the H abstraction reaction between a benzene molecule and a radical in the gas phase (Fig. 3).

Figure 3: Surface and gas phase prototype reactions.

This assumption was used since several publications related to the determination of kinetic data of reactions involving polycyclic aromatic hydrocarbon have shown that the kinetic rate of a class of reactions involving PAH is not dependent of the size of the considered PAH [28-30]. That's why only the reaction path degeneracy (RPD) is taken into account to estimate the pre-exponential factor of the reactions describing the growth of pyrocarbon, whereas activation energies are supposed to be similar for both the surface and prototype elementary steps.

In order to perform modelling, the surface site density and the contact area between carbon fibers and the gas phase are also required parameters. The area of the fibers has been estimated equal to 3960 cm^2 by the mean of geometric considerations and it is supposed to be constant during an experiment because of the short deposit rate. The surface site density on which deposition reactions occur is supposed to be equal to $8x10.^{14}$ $sites.cm^{-2}$, since it is the common value used in the modeling of deposit reactions on surfaces with a crystalline structure [31].

4. Influence of the hydrogen addition on the pyrocarbon deposition rate obtained by propane pyrolysis

The pyrocarbon deposition rate is presented in figure 4 as a function of the inlet hydrogen mole fraction in the reactor.

Figure 4: Pyrocarbon deposition rate as a function of the hydrogen mole fraction in the reactor inlet.

(◆ : experimental results, — : modeling results).

In accordance to previous observation the presence of hydrogen in the gas phase has an important inhibition effect on pyrocarbon deposition [11-15]. Indeed, the deposition rate of pyrocarbon is slower when the hydrogen mole fraction increases. Simulated results are coherent with experiments for hydrogen mole fractions in the reactor inlet ranging from 0 to 30%.

A flow rate and a sensitivity analysis were performed in the case of propane/hydrogen mixture pyrolysis to identify the major pyrocarbon precursors and the key deposition reactions. These results show that pyrocarbon is mostly formed by deposition of methyl radicals, acetylene and ethylene on boat sites, whereas the deposition of the other species such as C_3, aromatic and polyaromatic species can be neglected. Besides, the pyrocarbon deposition rate on zig-zag sites is very small compared to reactions on boat sites. These three deposition pathways are the main as those involved in the pyrolysis of pure propane [32-33]. They account for more than two third of the total pyrocarbon deposition rate and they are recalled in figures 5, 6 and 7; each reaction is followed by its reference number in the heterogeneous mechanism (Rx). They take place on boat sites and they make use of two carbon atoms in order to close a new ring. Methyl deposition involves in the first place a five carbons ring while acetylene and ethylene ways of deposition are quite similar. The methyl reactions of deposition are in fact close to that of isomerization between fulvene and benzene, since it allows the elimination of the five-membered ring in order to produce a new six-membered ring.

Figure 5: Deposition of methyl radicals on boat sites.

Figure 6: Deposition of acetylene on boat sites.

Figure 7: Deposition of ethylene on boat sites.

A sensitivity analysis on methyl, acetylene and ethylene has been also performed in the following conditions: a temperature of 1273K, a residence time of 1 second, a surface to volume ratio equals to 45cm^{-1}. The reactor inlet was composed of propane diluted in nitrogen with a mole ratio of 1/9. The results of this sensitivity analysis are presented in figure 8, they show the six key reactions involved in pyrocarbon deposition.

Figure 8: Sensitivity analysis on the three major pyrocarbon deposition pathways.

The X axis in figure 8 represents the sensitivity coefficient ci,j, which is calculated using equation 2, the corresponding reactions (Rx) are mentioned bellow the values of these coefficients.

$$c_{i,j} = \frac{\partial[\text{mole fraction of surface site "j"}]}{\partial[\text{kinetic rate of reaction "i"}]} \qquad (2)$$

The evolution of the pyrocarbon deposition rate as a function of the hydrogen mole fractions in the reactor inlet can be explained by the evolution of the deposition flow rates of methyl radicals, ethylene and acetylene on boat sites (figure 9). The three main pathways presented in figures 5, 6 and 7 are then concerned by the hydrogen inhibition.

Figure 9: Deposition flow rate of methyl radicals, acetylene and ethylene on boat sites as a function of the hydrogen mole fraction in the reactor inlet.

Indeed, the deposition rate of methyl radicals is controlled by reactions R(6), R(-4) and R(4) as it is shown in figure 8. When hydrogen is added in the reactor inlet, the mole fraction of H radicals in the gas phase increases whereas the mole fraction of CH_3 radicals decreases. This

can be explained by the metathesis reaction between methyl radicals with molecular hydrogen in the following homogeneous reaction:

$$CH_3 + H_2 \rightarrow CH_4 + H \qquad (3)$$

The net formation flow rate of methyl surface sites ($CH_3(S)$) consequently decreases when additional hydrogen is added in the reactor inlet. Indeed, these sites are produced and consumed mostly by the ipso-additions reactions R4/R-4 involving methyl radicals (presented in figure 8). This reaction R-4 is shifted towards the formation of surface hydrogen H(S) when hydrogen reactant is added in the reactor inlet.

Concerning the deposition of acetylene, it is also inhibited by hydrogen addition in the reactor inlet. According to the sensitivity analysis (figure 8), the deposition of C_2H_2 is controlled by creation and consumption reactions of carbon surface sites C.(S) (figures 6 and 8). These sites are created by hydrogen abstraction with H and CH_3 radicals (R1 and R2 in figure 8). The increase of the formation of C.(S) sites by a reaction with H atoms (reaction R1) is compensated by the decrease of the flow of the H-abstraction reaction with a methyl radical (reaction R2). The total formation flow rate of H-abstractions creating C.(S) surface sites is not affected by the addition of hydrogen in the reactor inlet. The consumptions pathways of C.(S) surface sites are however strongly influenced by the addition of hydrogen in the reactor inlet. Indeed, C.(S) surface sites are either consumed by an addition reaction with acetylene and ethylene or by a H-abstraction reaction with H_2. As the mole fraction of hydrogen in the gas phase increases, the fraction of C.(S) surface sites which are deactivated by the H-abstraction reaction increases as well. Less radical surface sites are therefore available for unsaturated species addition reactions. The inhibition of ethylene deposition (figure 7) by hydrogen addition in the reactor inlet is very similar to the inhibition of acetylene deposition.

The decrease of the C_2H_4 deposition flow rate is caused by the H-abstraction reaction between C.(S) and H_2, so by a deactivation of radical surface sites.

5. Influence of the hydrogen addition on the gas phase during pyrocarbon deposition obtained by propane pyrolysis

In this section, the influence of the addition of hydrogen in the reactor inlet on the mole fractions of major aliphatic and aromatic species in the gas phase is described. Since ethylene and acetylene are the main species involved in pyrocarbon deposition (as well as CH_3 radical), the effect of hydrogen on C_2 species and their by-products is analyzed. Hydrogen addition in the reactor inlet has almost no significant influence on mole fractions of acetylene and ethylene, both experimentally and by modeling (figure 10).

Figure 10: Mole fractions of acetylene and ethylene in the gas phase.

The fact that the ethylene and acetylene mole fractions do not depend on the hydrogen mole fractions in the reactor inlet indicates that the net formation rate of these two species is not affected by hydrogen addition in the gas phase. The pathways of ethylene formation in gas phase are presented in figure 11.

Figure 11: Formation pathways of ethylene molecule.

The ethylene formation flow rate is proportional to the amount of C_2H_5 and nC_3H_7 radicals in the gas phase. These two precursors are produced by propane decomposition (cleavage of a C-C bond) or by a hydrogen abstraction reaction by H atoms followed by an isomerization reaction in the case of $i\text{-}C_3H_7$ formation. When no hydrogen is added in the reactor inlet, the

relative decomposition rates of propane are 54%, 21% and 23% for pathways 1, 2 and 3 respectively (figure 11). Then, 94% of i-C_3H_7 radicals are transformed into n-C_3H_7 and 72% of these n-C_3H_7 radicals are in turns transformed into C_2H_4 molecules and CH_3 radicals, the other part forms C_3H_6 molecules. Consequently, 85% of propane are transformed into ethylene molecules and methyl radicals. When hydrogen is added in the reactor inlet, the flow rates of propane decomposition reactions remain almost constant. The production of ethylene molecules is, according to the flow rate analysis (figure 11), not affected by hydrogen addition in the reactor inlet. Regarding ethylene consumption reactions, over 90% of C_2H_4 molecules are consumed by hydrogen abstraction reactions with H and CH_3 radicals. When hydrogen is added in the reactor inlet, the mole fraction of H radicals increases whereas the mole fraction of methyl radicals decreases, because of the abstraction reaction between H_2 and CH_3 radicals (reaction III). As H radicals are more active than CH_3 radicals in H-abstraction reactions, the consumption flow rate of C_2H_4 (by simulation) slightly increase when hydrogen is added in the reactor inlet. This explains the slight decrease of simulated C_2H_4 mole fractions when hydrogen is added in the reactor inlet. H-abstraction reactions on ethylene molecules produce C_2H_3 radicals, which are easily transformed into acetylene and H atoms by a β-scission reaction. This consumption pathway represents around 90% of ethylene consumption reactions and almost does not depend on hydrogen mole fraction in the reactor inlet. The acetylene production flow rate is consequently not affected by hydrogen addition in the reactor inlet. Acetylene is a relatively stable molecule; the total consumption flow rate of C_2H_2 represents only around 20% of the pyrocarbon formation flow rate for hydrogen mole fractions in the reactor inlet ranging from 0 to 30%. In conclusion, the acetylene mole fraction in the gas phase is not affected by hydrogen addition in the reactor inlet, as its creation and consumption flow rates are not affected by H_2 addition.

Concerning the C_3 unsaturated species, their mole fractions as a function of the hydrogen mole fraction in the reactor inlet are presented in figure 12.

Figure 12: Mole fractions of C3 species in the gas phase as a function of the hydrogen mole fraction in the reactor inlet.

The mole fractions of the three considered species decrease significantly when hydrogen is added in the reactor inlet. Propene is produced by two "C-H" β-scission reactions involving nC_3H_7 and iC_3H_7 radicals (figure 11). As it was previously explained, when hydrogen is added in the reactor inlet, the mole fractions of H atoms increase because of the H-abstraction reaction between CH_3 radicals and H_2 (reaction 3). More propane molecules are consumed by H-abstraction reactions, producing n-C_3H_7 and i-C_3H_7 radicals. Nevertheless, the formation of C_3H_6 decreases by about 10% when the mole fraction of hydrogen in the reactor inlet is 30% compared to an experimentation realized without hydrogen addition. This decrease can be explained regarding consumption reactions of propene. Indeed, most of propene molecules are consumed by H-abstraction reactions with H radicals. As the amount of H radicals increases when hydrogen is added in the reactor inlet, the consumption flow of C_3H_6 increases as well. According to the flow rate analysis, the increase of the consumption reactions flow rates is more important than the increase of formation reactions flow rates. So, the mole fraction of propene in the gas phase consequently decreases when hydrogen is added in the reactor inlet. The decrease of the mole fractions of propyne and propadiene when hydrogen is added in the reactor inlet is a direct consequence of the evolution of propene mole fraction. Indeed these two C_3 species are produced from propene in two successive elementary steps (H- abstraction reaction followed by a β-scission).

The experimental and simulated mole fractions of benzene, phenylacetylene and phenylethylene are presented in figure 13.

Figure 13: Mole fractions of benzene, phenylethylene and phenylacetylene as a function of the hydrogen mole fraction in the reactor inlet.

The current gas phase model is inefficient to predict benzene mole fractions as a function of the hydrogen mole fraction in the reactor inlet. Experimentally, benzene quantity in the gas phase strongly decreases when hydrogen is added in the reactor, whereas the simulated results (figure 13) predict a constant benzene mole fraction. The variation between experimental and simulated results might be caused by the fact that simulated benzene formation flow rate is not sufficiently affected by hydrogen addition in the reactor inlet compared to experimental results. According to the flow rate analysis, benzene is formed by combination of two C_3H_3 radicals and by termination of a methyl radical on a cyclopentadienyl radical as it is shown in figure 14.

Figure 14: Pathways of benzene formation.

When hydrogen is added in the reactor inlet, the formation flow rate of C_3H_3 radicals decreases because the two precursors of this radical are propyne and propadiene. Consequently, the benzene formation flow rate by combination of two C_3H_3 radicals or via the formation of cyclopentadienyl radical, which is the main way, decreases when the mole fraction of H_2 increases. Regarding consumption reactions, 84% of benzene molecules react in hydrogen abstraction reactions with H and CH_3 radicals, producing phenyl radicals. Phenyl radicals are then consumed in H-abstraction reactions with H_2 or by addition of acetylene and

ethylene. When hydrogen is added in the reactor inlet, the proportion of phenyl radicals consumed by hydrogen abstraction reactions tends to increase whereas the proportion of phenyl radicals consumed in addition reactions tends to decrease, leading to lower styrene and phenylacetylene mole fractions in the gas phase. The acenaphtylene, naphthalene and indene mole fractions as a function of the hydrogen mole fraction in the reactor inlet are presented in figure 15.

Figure 15: Mole fractions of naphthalene, indene, and acenaphtylene as a function of the hydrogen mole fraction in the reactor inlet.

Concerning larger PAH, indene is mainly formed from the addition of benzyl radical on acetylene. Naphthalene is also a derivative of indene, because it is formed from indenyl radical. Finally naphthalene, via the addition of radical naphtyl on acetylene evolves to the formation of acenaphtylene. In these last three cases, we can observe light persistent differences between computed and experimental data which can be explained by the lack of some PAH pathways formation presented in the homogeneous part [21]. Besides, in our previous studies, some PAH were identified by GC-MS but they were not quantified and represented in the homogeneous mechanism [20-22]; nevertheless it has no influence on the pyrocarbon deposition mechanism.

6. Conclusion

Based on a detailed kinetic mechanism modeling both pyrocarbon deposition and gas phase composition obtained by propane pyrolysis on carbon fibers, the influence of hydrogen and its inhibiting effects on pyrocarbon deposition have been discussed. The aim of this paper was also to complete the knowledge of the influence of hydrogen mole fractions in the gas phase

and on pyrocarbon deposition. In order to validate this mechanism and this study, a quantitative experimental study of a propane/hydrogen mixture pyrolysis at high temperature (1273 K) and low pressure has been carried out in a self-stirred reactor. This reactor has the great advantage of having the same gaseous composition in all its volume, and allows to know precisely the composition of the gas phase where the pyrocarbon deposition takes place and in the pyrolysis conditions. Gas chromatography analyses (TCD/FID/MS) have allowed the quantification of more than 25 light and heavy species from methane up to pyrene, whereas the deposition rate of pyrocarbon is evaluated by weighing. Most of the results obtained by modeling correctly reproduce the experimental results on a wide range of hydrogen inlet composition (0-30%). With an addition of an important part of hydrogen (10% of propane; 0-30% of hydrogen), it was observed that the mole fractions of C_2 and C_4 species are not affected by the presence of H_2, whereas pyrocarbon deposition rate and mole fractions of C_3 and aromatic species decrease; these observations can be explained with a flow rate analysis of propane/hydrogene pyrolysis. The main result of this work confirms that hydrogen inhibits the formation of pyrocarbon and aromatic species and but it also allows the understanding of the main keys involved in the hydrogen inhibition. At last, the way of formation of the heaviest species in our homogeneous mechanism could be improved because only a little part of their formation and consumption is written; indeed it would be interesting to improve the agreement between computed and experimental. Nevertheless most of the results obtained with the homogeneous and heterogeneous model, and presented here, reproduce correctly the experimental results on a wide range of temperature, residence time, inlet composition and fibers surface (A/V ratio). Finally, it is worth noting that this agreement has been obtained with the same set of kinetic parameters and without any adjustment.

Acknowledgments

The authors wish to thank Herakles for financial and scientific support, and especially Sébastien Bertrand, Eric Bouillon, Cédric Descamps, Christian Robin-Brosse and Jacques Thébault.

Bibliography

1. Z.J. Hu, W.G. Zhang, K.J. Huttinger, B. Reznik, D. Gerthsen, Influence of pressure, temperature and surface area/volume ratio on the texture of pyrolytic carbon deposited from methane, Carbon 41 (2003) 749-758.

2. W. Benzinger, K.J. Hüttinger, Chemical vapor infiltration of pyrocarbon-II. The influence of increasing methane partial pressure at constant total pressure on infiltration rate and degree of pore filling, Carbon 36 (1998) 1033-1042.

3. C. Descamps, G. Vignoles, O. Féron, F. Langlais, J. Lavenac, Correlation between homogeneous propane pyrolysis and pyrocarbon deposit, J. Electrochem. Soc.148 (2001) 695-708.

4. Z.J. Hu, W.G. Zhang, K.J. Hüttinger, B. Reznik, D. Gerthsen, Influence of pressure, temperature and surface area/volume ratio on the texture of pyrolytic carbon deposited from methane, Carbon 41 (2003) 749-758.

5. R. Lacroix, R. Fournet, I. Ziegler-Devin, P.M. Marquaire, Kinetic modeling of surface reactions involved in CVI of pyrocarbon obtained by propane pyrolysis, Carbon 48 (2010) 132-144.

6. CY Lu, LF Cheng, LT Zhang, CN Zhao, Reaction kinetic in the CVD process of pyrocarbon deposition from propylene pyrolysis, International Workshop on Materials for Energy Conversion and Storage, Shenzhen, (2012)

7. K. Norinaga, V.M. Janardhanan, O. Deutschmann, Detailed chemical kinetic modeling of pyrolysis of ethylene, acetylene, and propylene at 1073-1373 K with a plug-flow reactor model, Int. J. Chem. Kinet. 40 (2008) 199-208.

8. A. Li, S. Zhang, B. Reznik, S. Lichtenberg, O. Deutschmann, Synthesis of pyrolytic carbon composites using ethanol as precursor, Ind. Eng. Chem. Res. 49 (2010) 10421-10427.

9. R. Naslain, F. Langlais, Fundamental and practical aspects of the chemical vapor infiltration of porous substrates, High Temperature Science 27 (1990) 221-235.

10. C. Descamps, G. Vignoles, O. Féron, J. Lavenac, F. Langlais, Kinetic modelling of gas-phase decomposition of propane: correlation with pyrocarbon deposit, J.Phys. IV 11 (2001) 101-118.

11. A. Li, K. Norinaga, O. Deutschmann, Modelling and simulation of materials synthesis: chemical vapor deposition and infiltration of pyrolytic carbon. European Conference on Computational Fluid Dynamics (ECCOMAS CDF 2006) Delft, the Netherland, Sept 5-8, 2006.

12. A. Li, O. Deutschmann, Transient modeling of chemical vapor infiltration of methane using multi-step reaction and deposition models, Chem. Eng. Sci. 62 (2007) 4976-4982.

13. A. Li, K. Norinaga, W. Zhang, O. Deutschmann, Modeling and simulation of materials synthesis: Chemical vapor deposition and infiltration of pyrolytic carbon, Comp Sci Tech, 68 (2008) 1097-1104.

14. A. Becker, Z. Hu, K. Huttinger, A hydrogen inhibition model of carbon deposition from light hydrocarbons, J. Fuel 79 (2000) 1573-1580.

15. Z.H. Tang, D.N. Qu, J. Xiong, Z.Q. Zou, Effects of infiltration conditions on the densification behavior of carbon/carbon composites prepared by a directional-flow thermal gradient CVI process, Carbon 41 (2003) 2703-2710.

16. D. G. Goodwin, J. E. Butler, Handbook of industrial diamonds and diamond films. Prelas G.P.M.A, Bigelow L.K Eds. New York, NY: Marcel Dekker, Inc. 1997, 527-581.

17. E.C. Sanford, Mechanism of coke prevention by hydrogen during residuum hydrocracking, Abstracts of papers of the American Chemical Society, 205 (1993) 47-48.

18. M. Frenklach, the role of hydrogen in vapour deposition of diamond, J. Appl. Phys. 65 (1989) 5142-5149.

19. M. Frenklach, Preprint, 197th ACS National Meeting, ACS, Division of Fuel Chemistry, Dallas, Texas, April 9-14, 1989.

20. I. Ziegler, R. Fournet, P.M. Marquaire, Influence of surface on chemical kinetic of pyrocarbon deposit obtained by propane pyrolysis, J. Anal. Appl. Pyrol. 73 (2005) 107-115.

21. I. Ziegler, R. Fournet, P.M. Marquaire, Pyrolysis of propane for CVI of pyrocarbon: Part I. Experimental and modeling study of the formation of toluene and aliphatic species, J. Anal. Appl. Pyrol. 73 (2005) 212-230.

22. I. Ziegler, R. Fournet, P.M. Marquaire, Pyrolysis of propane for CVI of pyrocarbon : Part II. Experimental and modeling study of polyaromatic species, J. Anal. Appl. Pyrol. 73 (2005) 231-247.

23. I. Ziegler, R. Fournet, P.M. Marquaire, Pyrolysis of propane for CVI of pyrocarbon. Part III: Experimental and modeling study of the formation of pyrocarbon, J. Anal. Appl. Pyrol. 79 (2007) 268-277.

24. D. Matras, J. Villermaux, Continuous reactor perfectly agitated by gas jets for kinetic study on rapid chemical reaction, J. Chem. Eng. Sci. 28 (1973) 129-137.

25. V. Bloch-Michel, Ph.D. thesis, Institut National Polytechnique de Lorraine, Nancy (1995).

26. J. Troë, Fall-off curves of unimolecular reactions, Ber. Bunsenges Phys. Chem.78 (1974) 478-488.

27. C. Muller, V. Michel, G. Scacchi, M. Côme, THERGAS. A computer program for thermochemical evaluation data of molecules and free radicals in the gas phase, J. Chim. Phys. 92 (1995) 1154-1178.

28. K. Hemelsoet, V. Van Speybroeck, D. Moran, G.B. Marin, L. Radom, M. Waroquier, Thermochemistry and kinetics of hydrogen abstraction by methyl radical from polycyclic aromatic hydrocarbons, J. Phys. Chem. A 110 (2006) 13624-13631.

29. A. Violi, T.N. Truong, A.F. Sarofim, Kinetics of hydrogen abstraction reactions from polycyclic aromatic hydrocarbons by H atoms, J. Phys. Chem. A 108 (2004)4846-4852.

30. I.V. Tokmakov, M.C. Lin, Reaction of phenyl radicals with acetylene: quantum chemical investigation of the mechanism and master equation analysis of the kinetics, J. Am. Chem. Soc. 125 (2003) 11397-11408.

31. M. Frenklach, H. Wang, Detailed surface and gas-phase chemical kinetics of diamond deposit, Phys. Rev. B: Condens. Matter. 43 (1991) 1520-1545.

32. R. Lacroix, R. Fournet, I. Ziegler-Devin, P. M. Marquaire, Major Precursors of Pyrocarbon Deposition from Propane Pyrolysis, ECS Trans 2009, 25, 91-98.

33. I. Ziegler-Devin, R. Fournet, R. Lacroix, P. M. Marquaire, Pyrolysis of propane for CVI of pyrocarbon. Part IV: Main pathways involved in pyrocarbon deposit, J. Anal. Appl. Pyrol. 104 (2013) 48-58.

Table 1: Hydrogen inhibition functions of a global deposition model proposed by Li et al. (2008).

Species	Preexponential factor A (m/s)	Activation energy ($kJ.mol^{-1}$)	Hydrogen inhibition function fi.
C_2H_4	7.24E+01	155.0	$1.104/\left(1.104+\frac{[H_2]}{[C_2H_4]}\right)$
C_2H_2	1.35E+01	126.0	$3.269/\left(3.269+\frac{[H_2]}{[C_2H_2]}\right)$
C_6H_6	4.71E+05	217.0	$0.5887/\left(0.5887+\frac{[H_2]}{[C_6H_6]}\right)$

Figure captions

Fig. 1 - Multi-step CVD and hydrogen inhibition of pyrocarbon from methane proposed by Li et al. (2008).

Fig. 2 - Zig-zag and armchair surface sites.

Fig. 3 - Surface and gas phase prototype reactions.

Fig. 4 - Pyrocarbon deposition rate as a function of the hydrogen mole fraction in the reactor inlet (◆ : experimental results, ── : modeling results).

Fig. 5 - Deposition of methyl radicals on boat sites.

Fig. 6 - Deposition of acetylene on boat sites.

Fig. 7 - Deposition of ethylene on boat sites.

Fig. 8 - Sensitivity analysis on the three major pyrocarbon deposition pathways.

Fig. 9 - Deposition flow rate of methyl radicals, acetylene and ethylene on boat sites as a function of the hydrogen mole fraction in the reactor inlet.

Fig. 10 - Mole fractions of acetylene and ethylene in the gas phase.

Fig. 11 - Formation pathways of ethylene molecule.

Fig. 12 - Mole fractions of C3 species in the gas phase as a function of the hydrogen mole fraction in the reactor inlet.

Fig. 13 - Mole fractions of benzene, phenylethylene and phenylacetylene as a function of the hydrogen mole fraction in the reactor inlet.

Fig. 14 - Pathways of benzene formation.

Fig. 15 - Mole fractions of naphthalene, indene, and acenaphtylene as a function of the hydrogen mole fraction in the reactor inlet.

Fig. 1 - Multi-step CVD and hydrogen inhibition of pyrocarbon from methane proposed by Li et al. (2008).

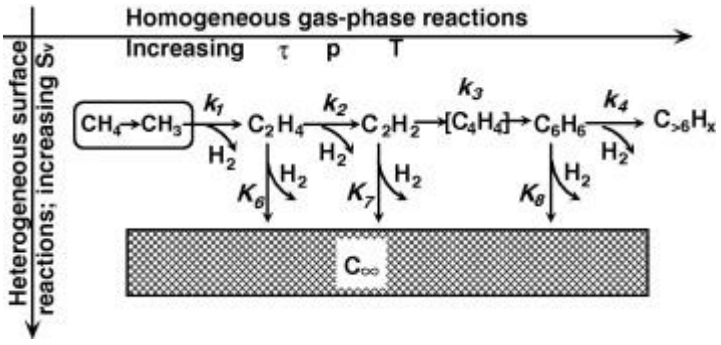

Fig. 2 - Zig-zag and armchair surface sites.

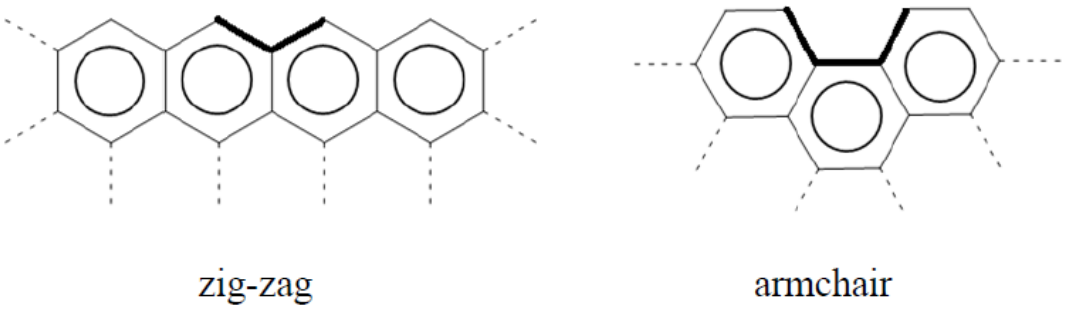

Fig. 3 - Surface and gas phase prototype reactions.

Reaction occurring at the surface :

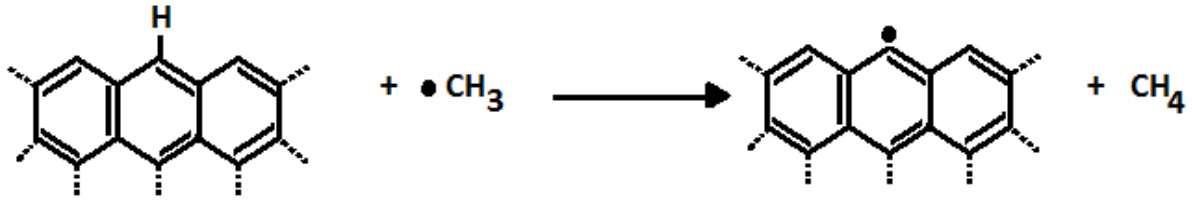

Corresponding gas phase reaction (prototype reaction) :

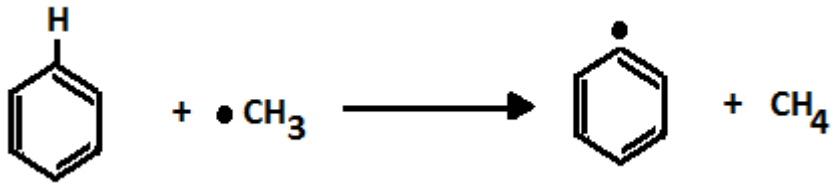

Fig. 4 - Pyrocarbon deposition rate as a function of the hydrogen mole fraction in the reactor inlet

(◆ : experimental results, ── : modeling results).

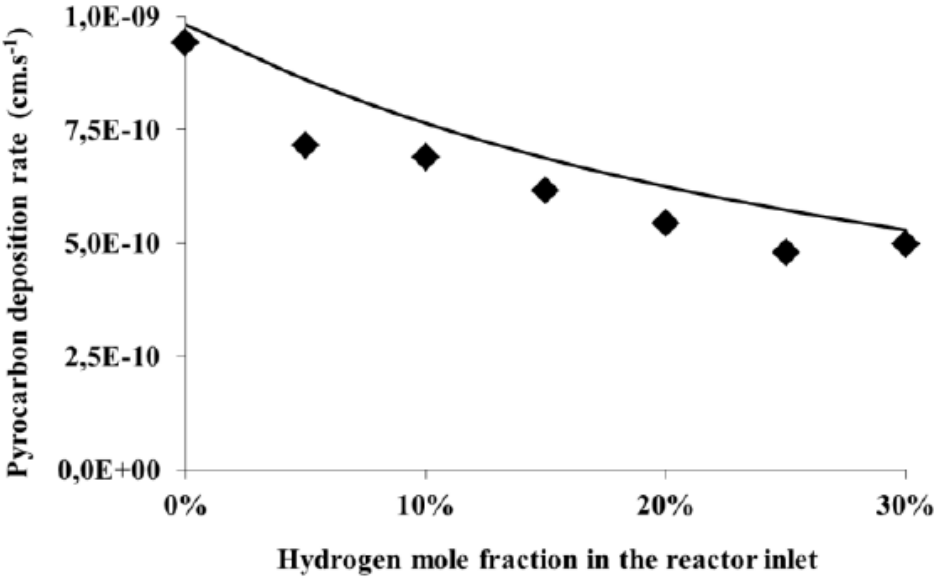

Fig. 5 - Deposition of methyl radicals on boat sites.

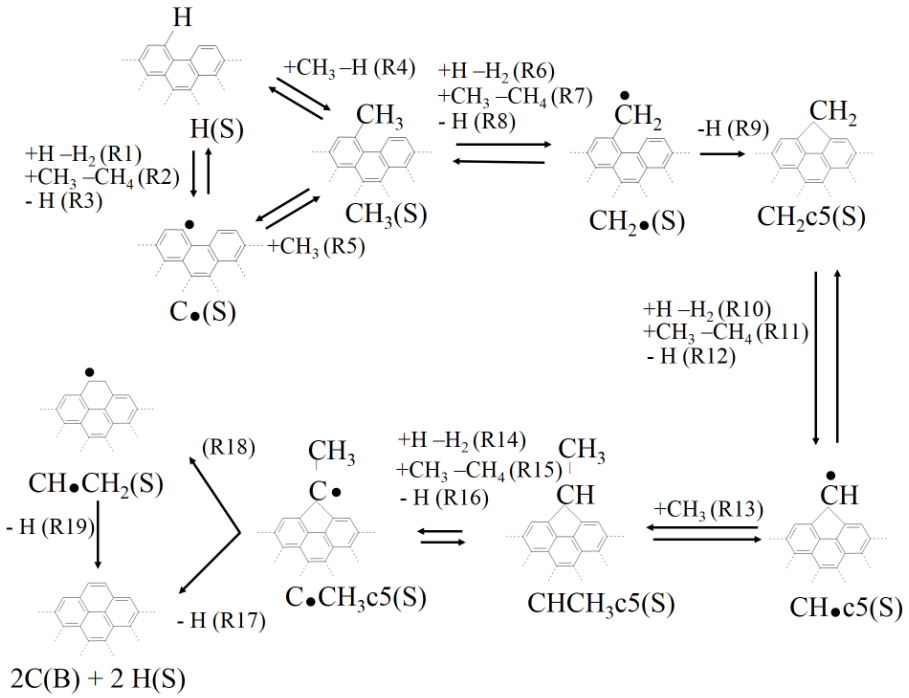

Fig. 6 - Deposition of acetylene on boat sites.

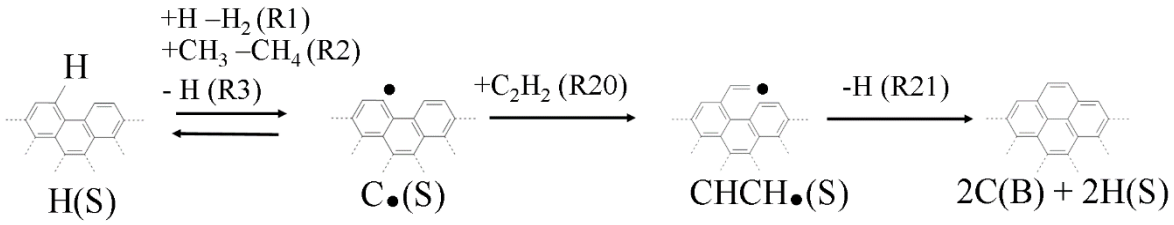

Fig. 7 - Deposition of ethylene on boat sites.

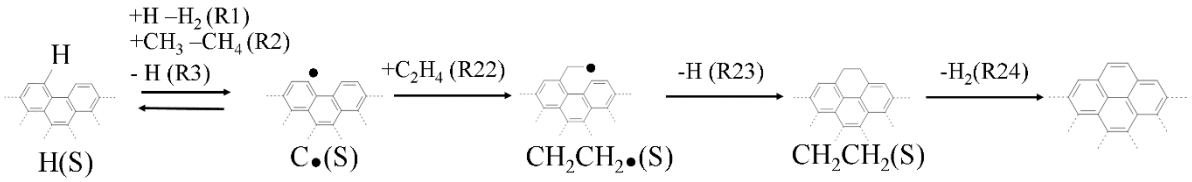

Fig. 8 - Sensitivity analysis on the three major pyrocarbon deposition pathways.

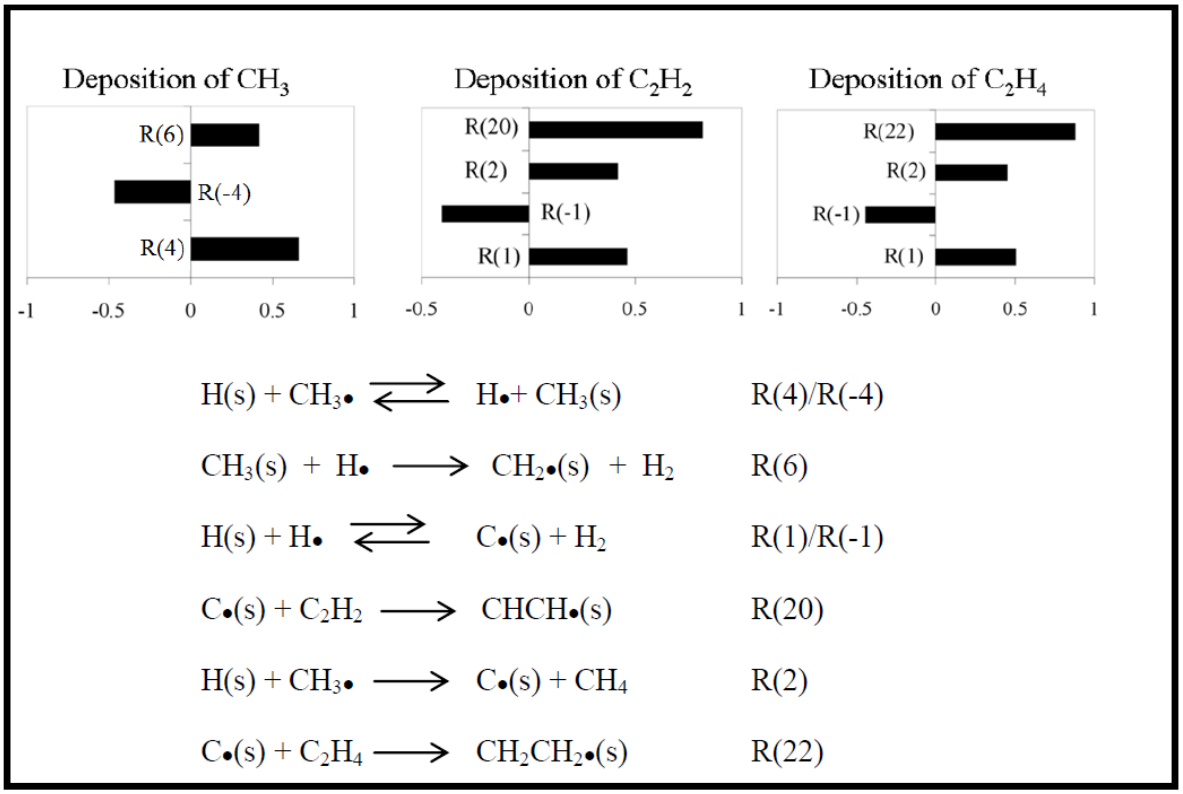

Fig. 9 - Deposition flow rate of methyl radicals, acetylene and ethylene on boat sites as a function of the hydrogen mole fraction in the reactor inlet.

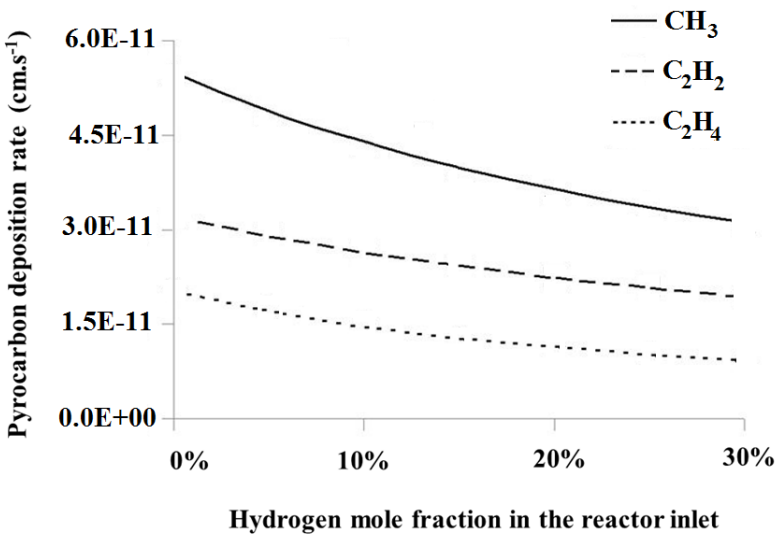

Fig. 10 - Mole fractions of acetylene and ethylene in the gas phase.

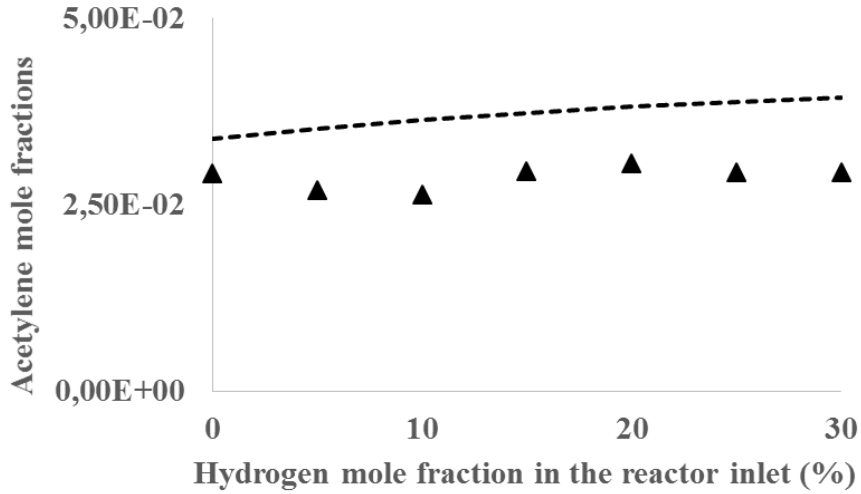

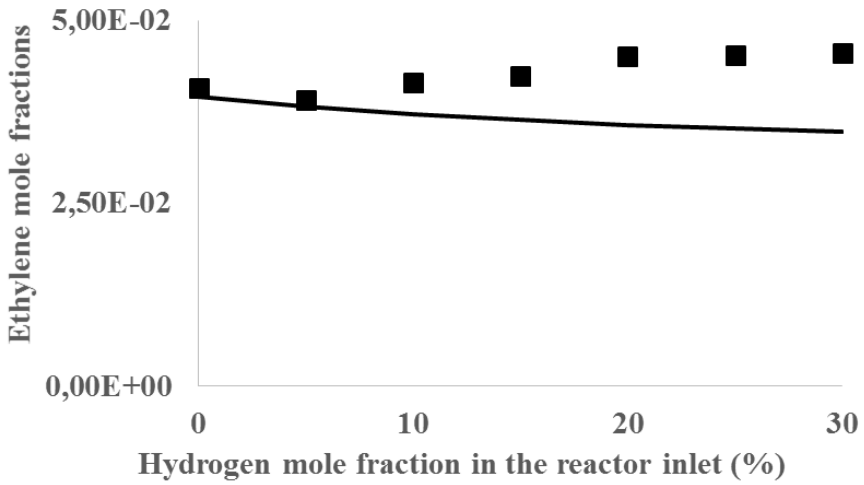

Fig. 11 - Formation pathways of ethylene molecule.

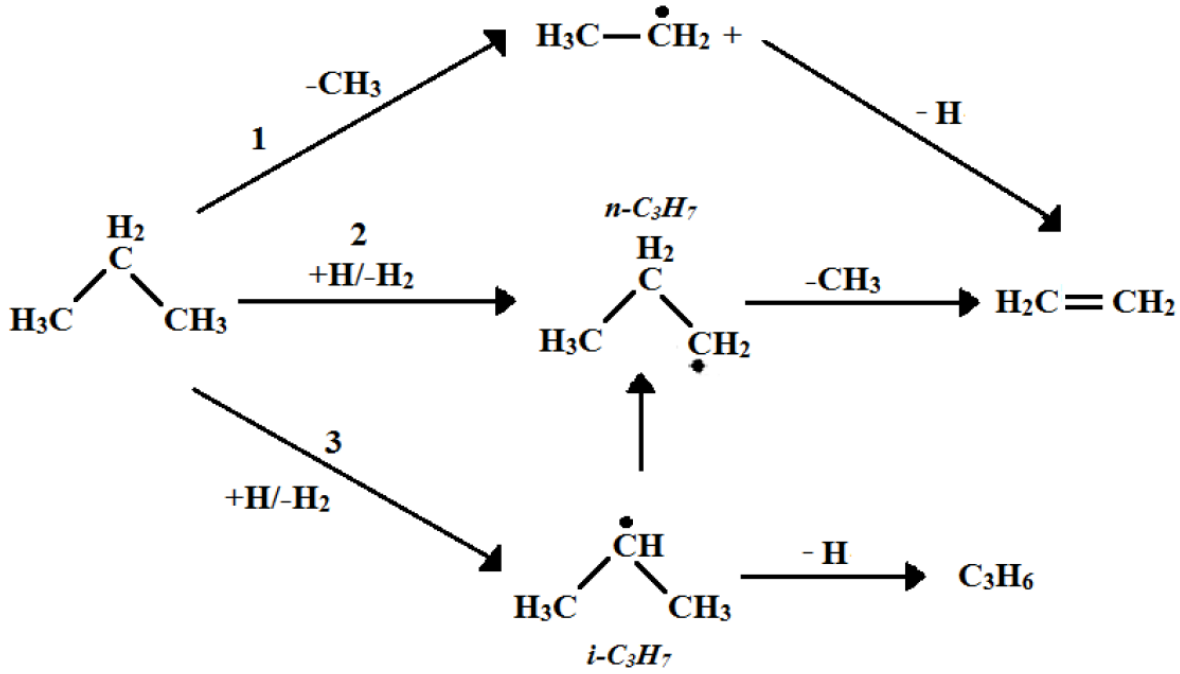

Fig. 12 - Mole fractions of C3 species in the gas phase as a function of the hydrogen mole fraction in the reactor inlet.

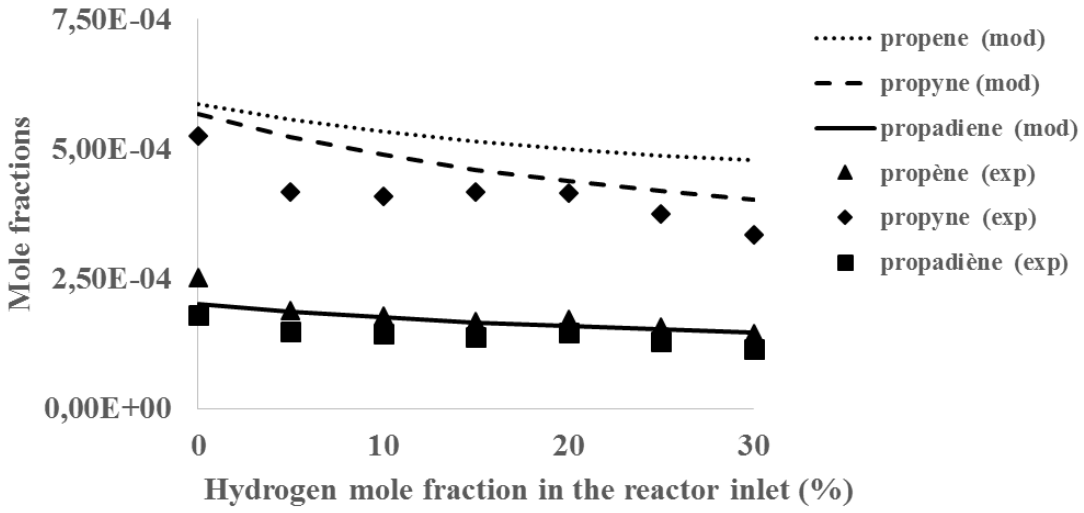

Fig. 13 - Mole fractions of benzene, phenylethylene and phenylacetylene as a function of the hydrogen mole fraction in the reactor inlet.

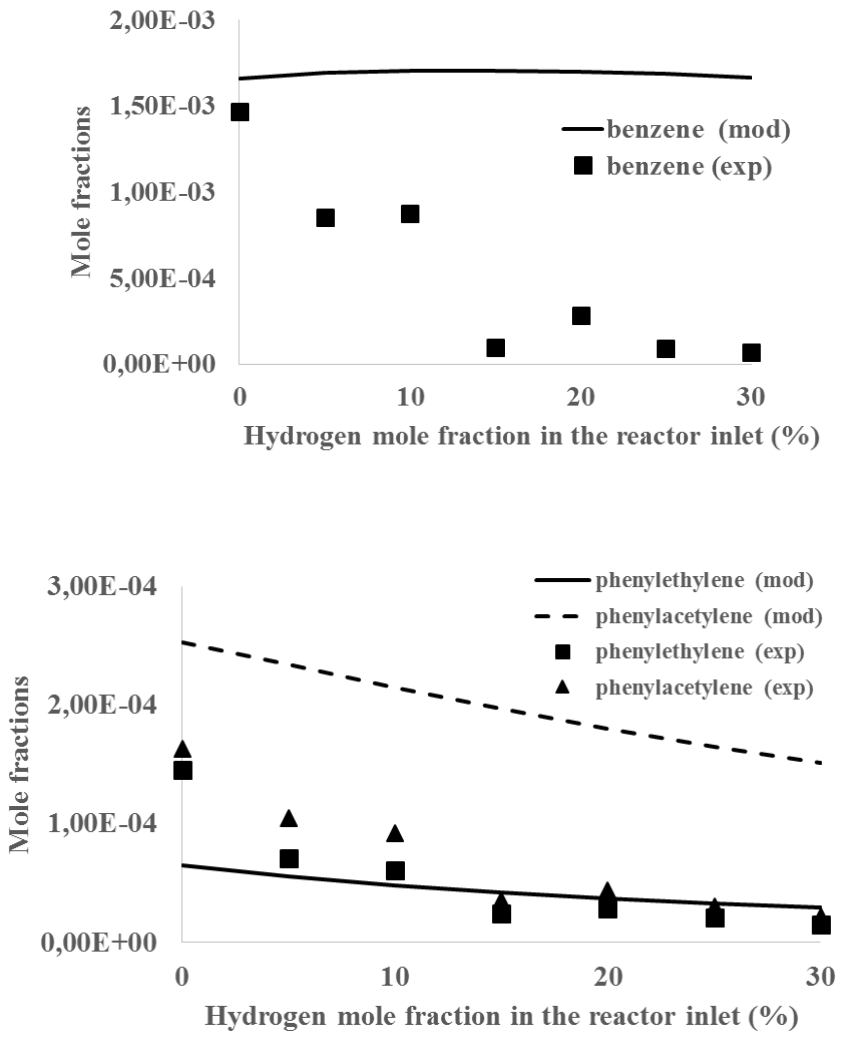

Fig. 14 - Pathways of benzene formation.

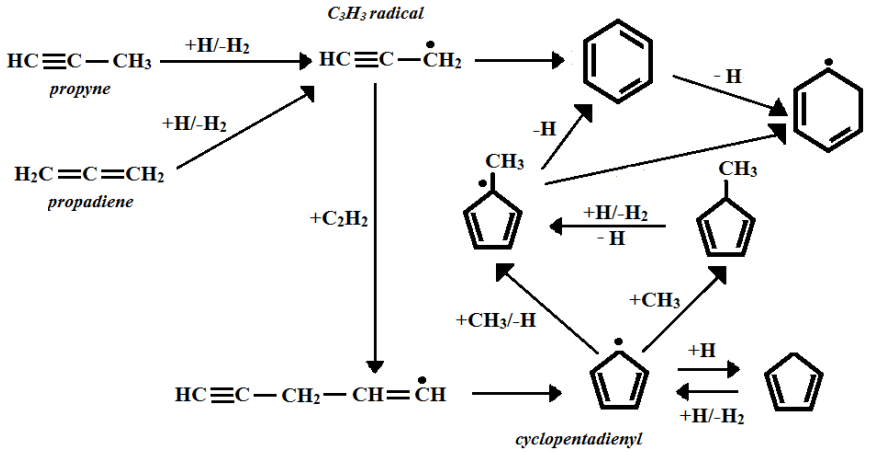

Fig. 15 - Mole fractions of naphthalene, indene, and acenaphtylene as a function of the hydrogen mole fraction in the reactor inlet.